SEGMENTATION-FREE AND MULTISCALE-FREE EXTRACTION OF MEDIAL INFORMATION USING GRADIENT VECTOR FLOW - APPLICATION TO VASCULAR STRUCTURES

Guillaume Pizaine[1, 2] *Raphael Prevost*[1,3] *Elsa D. Angelini*[2] *Isabelle Bloch*[2] *Sherif Makram-Ebeid*[1]

[1] Medisys Research Lab, Philips Healthcare, Suresnes, France.
[2] Institut Telecom, Telecom ParisTech, CNRS LTCI, Paris, France.
[3] CEREMADE, UMR 7534 CNRS, Paris Dauphine University, Paris, France.

ABSTRACT

Gradient Vector Flow has become a popular method to recover medial information in medical imaging, in particular for vessels centerline extraction. This renewed interest has been motivated by its ability to process gray-scale images without prior segmentation. However, another interesting property lies in the diffusion process used to solve the underlying variational problem. We propose a method to recover scale information in the context of vascular structures extraction, relying on analytical properties of the Gradient Vector Flow only, with no multiscale analysis. Through simple one-dimensional considerations, we demonstrate the ability of our approach to estimate the radii of the vessels with an error of 10% only in the presence of noise and less than 3% without noise. Our approach is evaluated on convolved bar-like templates and is illustrated on 2D X-ray angiographic images.

***Index Terms*—** gradient vector flow, diffusion, medialness, skeleton, shape analysis

1. INTRODUCTION

Gradient Vector Flow (GVF) has first been introduced as an external force field for active contours and active surfaces by Xu et al. [1]. The GVF of an image is the vector field obtained by diffusing its gradients in homogeneous regions while keeping strong gradients untouched. The diffusion process spreads edge information into uniform regions and acts as a long range force (see Fig. 2). Consequently, it also introduces more robustness against initialization and speeds up convergence.

Formally, the GVF of an image I over a domain Ω is defined as the global minimizer $\boldsymbol{V}$ of the following energy functional E:

$$E = \int_{\Omega} \left(g(\boldsymbol{x}) \parallel \nabla \boldsymbol{V} \parallel^2 (\boldsymbol{x}) + h(\boldsymbol{x}) |\boldsymbol{V}(\boldsymbol{x}) - \nabla I(\boldsymbol{x})|^2 \right) \mathrm{d}\boldsymbol{x} \,, \quad (1)$$

where $g : \Omega \to \mathbb{R}$ and $h : \Omega \to \mathbb{R}$ are spatially-varying weighting functions and $\parallel \nabla \boldsymbol{V} \parallel$ is the vector norm for tensors given by $\sqrt{\nabla \boldsymbol{V} . \nabla \boldsymbol{V}}$. The first term is a regularization term that controls the diffusion over the whole image domain. The second term is a data attachment term which ensures that $\boldsymbol{V}$ is close to the image gradient at strong edges. This is the General Gradient Vector Field (GGVF) devised by Xu et al. [2], which comes down to the original formulation of the GVF [1] if g is constant and $h(\boldsymbol{x}) = |\nabla I(\boldsymbol{x})|^2$. The most widely used functions are $g(\boldsymbol{x}) = e^{-|\nabla I(\boldsymbol{x})|/K}$, $K \in \mathbb{R}^*$ and $h(\boldsymbol{x}) = 1 - g(\boldsymbol{x})$, and will be used in this paper too. Since both GVF and GGVF formulations yield similar results, we will use the term GVF in the remaining of the paper.

The first variation of the functional E yields the following Euler-Lagrange equation[1]:

$$g(\boldsymbol{x}) \Delta v_i(\boldsymbol{x}) - h(\boldsymbol{x})(v_i(\boldsymbol{x}) - \nabla I(\boldsymbol{x})) = 0 \ , \quad (2)$$

where v_i is the i-th component of the vector field and Δ is the Laplacian operator.

Recently, GVF has become popular in the field of medial information extraction. Many ways of using it have been proposed since it can be viewed as an improved gradient vector field to compute various features. For instance, Bauer et al. [3] propose to recover the centerlines of airways by computing the Hessian matrix from the GVF. Then, they determine the cross-sectional planes of the tubular structures and compute a tube-likeliness map from flux measures in those planes, based again on the GVF. Flux measures were also used by Engel et al. [4] for medial features detection. Several previous works also exhibit GVF-based medialness maps derived from observations. Among them, the tube-likeliness from Bauer et al. [5] has already been mentioned. Yu et al. [6] propose to build a skeleton strength map from the GVF norm for gray-scale image segmentation. Finally, the GVF has also been used to extract skeletons from binary shapes. In this context, the GVF is used by Hassouna et al. [7] in a front propagation setting to design a speed function allowing faster propagation at the center of structures.

Although the GVF has already been used to extract medial information, few approaches have been proposed to recover scale information. Unlike multiscale filters, which retain the maximum response over several scales, the GVF diffuses information without keeping track of the scale. Although one benefits from this by freeing oneself from scale constraints (e.g. Hessian matrices can be computed on a 3x3 neighborhood only), scale information is still of paramount importance for skeletons or medialness maps. Knowing the centerlines, the method by Bauer et al. [3] goes back to the airways wall by tracking the GVF back to the edges in the image, which is quite time-consuming. Engel et al. [4] recover the size of the structures as the radius yielding a maximal circular (or spherical) flux. It seems to contradict the multiscale-free approach of the GVF.

In this paper, we propose a simple, segmentation-free and multiscale-free algorithm to extract medial information from images, based on the GVF. Since our approach heavily relies on 1-D analysis of the GVF (line by line in different directions), Sect. 2 gives a thorough review of the analytic solution for the 1-D case. Section 3 details the algorithm, especially how scale information is

[1] As stated by Xu et al. [2], the calculus of variations yields a third term $\langle \nabla g(\boldsymbol{x}), \nabla v_i \rangle$ in the corresponding Euler-Lagrange equation, which does not change the result much in practice.

recovered. Finally, we discuss parameters and show results on 2D angiographic images in Sect. 4.

2. ANALYTICAL SOLUTION FOR THE ONE-DIMENSIONAL CASE

Equation 2 is a diffusion-reaction equation whose analytical solution is not obvious without further assumptions on h and g (as defined in Sect. 1). For a better understanding, we will first focus on the 1-D case. We consider vessel edges as ramps which lead to plateau-like patterns in the original gradient (Fig. 1). A bar-like convolved model approximates well a vessel profile, but the influence of the convolution is limited in practice (see Sect. 4.1). The equation is decomposed and can be solved onto subdomains $\{\Omega_k\}_{0\leq k\leq N}$ where g_k and h_k, the restrictions of g and h to Ω_k, are constant. In the following developments, f_k will denote the restriction of any function f to Ω_k.

Two cases arise. If Ω_k is a homogeneous region, $\nabla I_k = 0$ so $g_k(\boldsymbol{x}) = 1$ and $h_k(\boldsymbol{x}) = 0$. Equation 2 is then the 1-D heat equation $\frac{\partial^2 V_k}{\partial x^2} = 0$, and the solution is a linear function:

$$V_k(x) = m_k x + p_k \;, \quad m_k, p_k \in \mathbb{R} \;. \tag{3}$$

If Ω_k is a region where the gradient is non-zero, then ∇I_k is constant (with the ramp model) and so are g_k and h_k. Equation 2 has then the form:

$$\frac{\partial^2 V_k}{\partial x^2} - a^2(V_k - \frac{\partial I}{\partial x}) = 0\,, \quad a^2 = \frac{1-g_k}{g_k}\,, \quad 0 < g_k \leq 1 \;. \tag{4}$$

Solutions to this second order linear equation with constant coefficients are of the form $V_k(x) = c_k^{(1)} e^{ax} + c_k^{(2)} e^{-ax} + b(x)$, where $c_k^{(1)}, c_k^{(2)} \in \mathbb{R}$ and b is a particular solution. Since ∇I is constant over Ω_k, it satisfies the equation. Finally, the solutions on such subdomains are of the form:

$$V_k(x) = c_k^{(1)} e^{ax} + c_k^{(2)} e^{-ax} + \nabla I(x) \;. \tag{5}$$

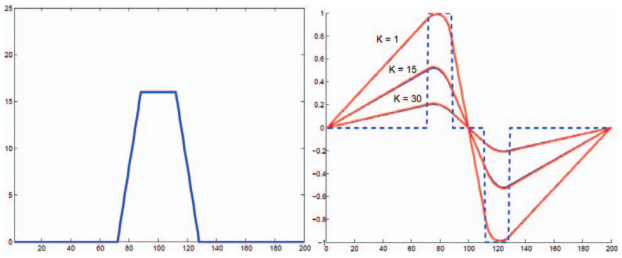
The parameters $m_k, p_k, c_k^{(1)}$ and $c_k^{(2)}$ for each subdomain Ω_k are given by the Dirichlet boundary condition $V = 0$ on $\partial\Omega$ and the $\mathcal{C}^0$ and $\mathcal{C}^1$ properties of the global solution V at boundaries between the N subdomains. This yields the following linear system (in the same order):

$$\begin{aligned} p_1 &= 0 \\ m_N x_N + p_N &= 0 \\ m_{k-1} x_k + p_{k-1} &= c_k^{(1)} e^{a x_k} + c_k^{(2)} e^{-a x_k} + V_k(x_k) \\ m_{k+1} x_{k+1} + p_{k+1} &= a c_k^{(1)} e^{a x_{k+1}} - a c_k^{(2)} e^{-a x_{k+1}} \;, \end{aligned} \tag{6}$$

where x_i denotes the point limiting Ω_{i-1} and Ω_i, and $0 < k < N$. If there are M plateau-like patterns, this yields a linear system of $4M+2$ equations. A numerical solution and the corresponding analytical solution, computed from a two ramps gradient, are illustrated in Fig. 1. In practice, subdomains Ω_k where $\nabla I \neq 0$ tend towards $\varnothing$, which means that the GVF can be approximated by a piecewise-linear function. Although this is a mere approximation, we will use this property to derive our scale measure.

3. DETECTION OF MEDIAL POINTS AND THEIR CORRESPONDING SCALE

The GVF energy functional in Eq. 1 contains a diffusion term which is equivalent to a multiscale analysis, from a scale-space point of view. The method proposed here is driven by two ideas. First, scale information should be available directly from the GVF, without any further multiscale analysis. Second, given the sophistication of the GVF, recovering scales should not use overcomplicated analysis schemes of the solution.



(a) (b)

Fig. 1: (a) Original signal and (b) the analytical solution of the GVF equation for $K = 3$, $K = 15$ and $K = 30$ (where K is the parameter of function g). The dotted line represents the original normalized gradient, the analytical solution is plotted in plain red, and the numerical solution is in plain blue. Both solutions overlap almost completely. The zero-crossings are preserved for all values of K but the positions of the maxima of the solutions are clearly impacted.

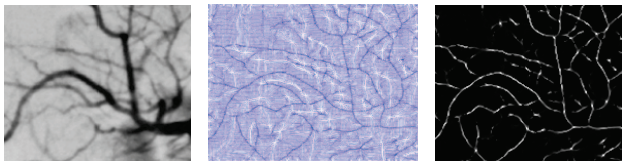
In contrast-enhanced images, vascular structures are considered as homogeneous regions surrounded by strong gradients. In those regions, gradients having opposite directions collide at the center of the structures because of the diffusion process. This interpretation still holds in the 1-D case: thanks to the separability property of the GVF, one can consider working on the projections of the solution $\boldsymbol{V}$ along each dimension instead of working on the gradient vector field itself. This means that analyzing the d-th component v_d of $\boldsymbol{V}$ along the d-th dimension only is relevant. In this outlook, the separability of the GVF and results from Sect. 2 are exploited both to detect medial points and to estimate the radius of vessel structures.

3.1. Detection of medial points

Associating gradients having opposite directions comes down to finding projections along each dimension d having opposite signs (see Fig. 1). According to Sect. 2, the GVF may be approximated by a linear function and vanishes between those two gradients. To ensure that zero-crossings happen in the center of structures, both corresponding gradients must have exactly the same magnitude. This is why we choose to diffuse the normalized image gradient.

In practice, the Point Spread Function (PSF) of the acquisition system interferes with the linearity of the solution inside homogeneous regions so that the slope of the solution $\boldsymbol{V}$ is weaker near edges. Along a given dimension d, medial points are thus detected as zero-crossings of the GVF components v_d, which can still be emphasized by taking the components $\tilde{v}_d$ of the normalized solution $\tilde{\boldsymbol{V}}$. Responses are summed over all dimensions to obtain the final measure for medial points (see Fig. 2(c)):

$$\mathcal{M} = \mathrm{div}(\tilde{\boldsymbol{V}}) = \sum_d \frac{\mathrm{d}\tilde{v}_d}{\mathrm{d}x_d} \;. \tag{7}$$



(a) (b) (c)

Fig. 2: (a) Original image, (b) normalized GGVF and (c) medialness map $\mathcal{M}$ from Eq. 7.

3.2. Estimation of the radius of the structures

Following the remarks formulated in the previous paragraph concerning the linear approximation, the slope of v_d is inversely proportional to the radius of the structures. Let $r_{d,k}$ be the size of the structures along dimension d, delimited by two gradients $v_d(x_k)$ and $v_d(x_{k+1})$ at positions x_k and x_{k+1}, corresponding to edges of a structure. The slope m_k can be recovered where v_d vanishes and the radius can be estimated as:

$$r_{d,k} = \frac{v_d(x_k) - v_d(x_{k+1})}{2m_k} \quad . \tag{8}$$

Knowing the positions x_k and x_{k+1} is not obvious. This is why previous works usually resort to an exhaustive search through multi-scale analysis. On the contrary, since we are able to detect structures (vessels or other structures) thanks to zero-crossings, we have all the necessary information to approximate v_d with a piecewise-linear function. We are only interested in the positions where two linear functions intersect. Thus, the approximation does not have to be accurate (see Fig. 3). A position x_k, at the boundary of linear regions Ω_k and Ω_{k+1} with corresponding zero-crossings c_k and c_{k+1}, is thus recovered as:

$$x_k = \frac{m_{k+1}c_{k+1} - m_k c_k}{m_{k+1} - m_k} \quad . \tag{9}$$

Note that the radii $r_{d,k}$ are computed only once for a range $[x_k; x_{k+1}]$. Thus, our algorithm scales well with the size of the image.

Under the assumption that the curvature of the vessel wall is locally small, the actual radius r_k can now be computed with simple geometrical considerations. For example, for 2D images where $d \in \{x, y\}$, the radius is:

$$r_k = r_{x,k} \sin \arccos \left(\frac{r_{x,k}}{\sqrt{r_{x,k}^2 + r_{y,k}^2}} \right) \quad . \tag{10}$$

The situation for a given medial point is summarized in Fig. 4. Finally, an additional smoothing of estimated radii is performed along the centerlines to increase the robustness.

4. EVALUATION OF THE ESTIMATED SCALES AND APPLICATION TO VASCULAR STRUCTURES

Equation 2 can be solved with various explicit, implicit or semi-implicit schemes. We implemented the common explicit scheme for simplicity (see [8] for more efficient explicit and implicit schemes). In particular, unconditionnally stable explicit schemes exist (the Alternating Direction Explicit scheme, for example). In practice, the straightforward explicit scheme is still widely used and is very useful for investigation. We recall the 1-D version of this scheme [2].

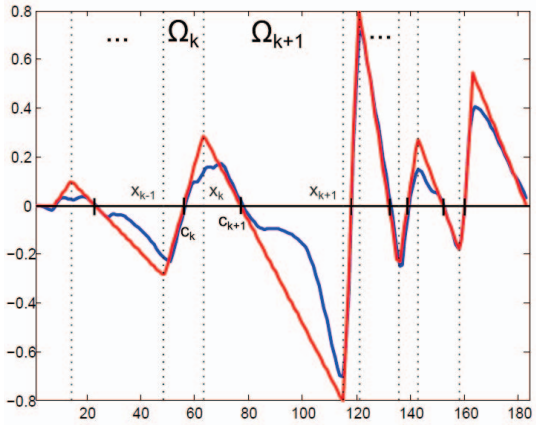


Fig. 3: Solution to the GVF (in blue) for a 1-D profile extracted from Fig. 2 and its corresponding piecewise linear reconstruction (in red).

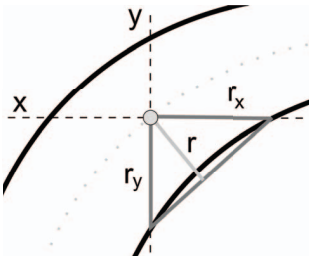


Fig. 4: Provided the curvature is small with respect to the vessel radius r, the latter can be approximated from the estimations r_x and r_y along each direction by simple geometric considerations.

If V_i^n is the value of the solution at point x_i after the n-th iteration, then:

$$V_i^{n+1} = (1 - h\Delta t)V_i^n + \frac{g\Delta t}{\Delta x}\left(V_{i-1}^n + V_{i+1}^n - 2V_i^n\right) + h\nabla I \Delta t \quad , \tag{11}$$

where Δx is the spatial resolution and Δt is the time step.

4.1. Validation on synthetical vessel templates

As mentioned in Sect. 3.1, the PSF of the acquisition system and partial volume effects impact the estimation of the vessels radius. To study their influence, we apply our algorithm to vessel templates with various radii and PSF. Vessels are modeled by convolved bar-like cross-sections with radii r^0 ranging from 1 to 25 pixels, and the scale of the convolution σ_{PSF} is set to 0.5, 1 and 2 pixels (we approximate the PSF by a Gaussian kernel).

The relative error of the estimation with respect to the ground truth $err(r) = \frac{|r - r^0|}{r^0}$ is illustrated in Fig. 5. The algorithm introduced in Sect. 3.2 is represented by blue lines. We compare it with two alternative approaches. The first one, represented by red lines, computes the radius by taking $r = \min(|x_k - c_k|, |x_{k+1} - c_{k+1}|)$. The second one, represented by the green lines, corresponds to the distance from c_k to the closest local maximum of $\| \boldsymbol{V} \|$. Finally, the evaluation was performed on noise-free profiles ($K = 5$) in the first line, and on profiles corrupted with a 10% random additive Gaussian noise ($K = 15$ to compensate for the presence of noise) in the second line.

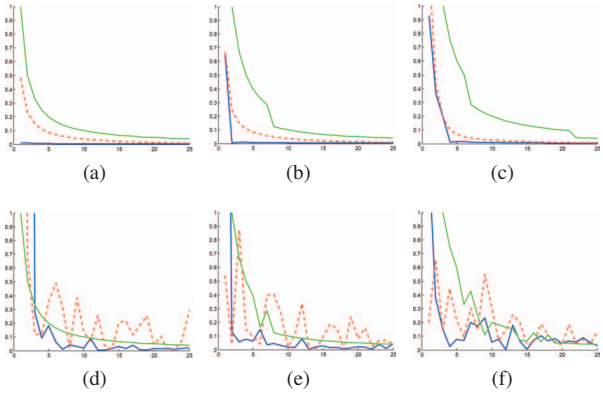


Fig. 5: Relative error *err* of the estimated radius for radii r^0 ranging from 1 to 25 pixels and a Gaussian PSF with (a,d) $\sigma_{PSF} = 0.5$, (b,e) $\sigma_{PSF} = 1$, (c,f) $\sigma_{PSF} = 2$. The first row shows the result for profiles with no noise, while a 10% random Gaussian noise has been added to vessel templates in the second row (see Sec. 4.1 for further details).

It is clear that our algorithm performs better for all PSF values and is globally more robust to noise. When $r^0 \leq \sigma_{PSF}$ with no noise, the estimation is clearly unreliable but usable since the error is still less than one pixel. For $r^0 > \sigma_{PSF}$, the error is less than 3% for noise-free profiles, and remains low (around 10%) in the presence of additive Gaussian noise . However, for radii smaller than the PSF, zero-crossings of the GVF may disappear and thus our algorithm fails to recover the structure, which corresponds to very high errors for small r^0 values in Fig. 5.

4.2. Skeleton extraction of vascular structures

Our algorithm was also tested to extract the skeleton of vascular structures in 2D angiographic images. The medialness map $\mathcal{M}$ from Eq.7 and the radii are computed from the 2D GVF of the image. Seed points are selected as directional maxima of $\mathcal{M}$ but discarded if they are in regions with low local contrast. Finally, centerlines are extracted as the ridges of $\mathcal{M}$ going through seed points, as in [9]. The centerlines and a segmentation reconstructed from the medial points and their radius are shown in Fig. 6. Most vessels are correctly recovered, with accurate radii (they are slightly overestimated in the case of very small vessels, as one should expect from Sect. 4.1).

5. CONCLUSION

We presented a new segmentation-free method to extract scale information of vascular structures from the GVF of an image, without any additional multiscale analysis. We demonstrated that, through fast and effective 1-D analysis of the GVF, we are able to devise a method which is both accurate and robust to noise. The result can serve as an input for deformable model-based algorithms, to further refine the segmentation. The current bottleneck of our approach lies in the computation of the GVF which is highly time-consuming, as any process involving diffusion. Efforts will be put on efficient schemes to solve the underlying variational problem. In the future, we believe that our approach will prove to be a good alternative to multiscale vessel analysis.

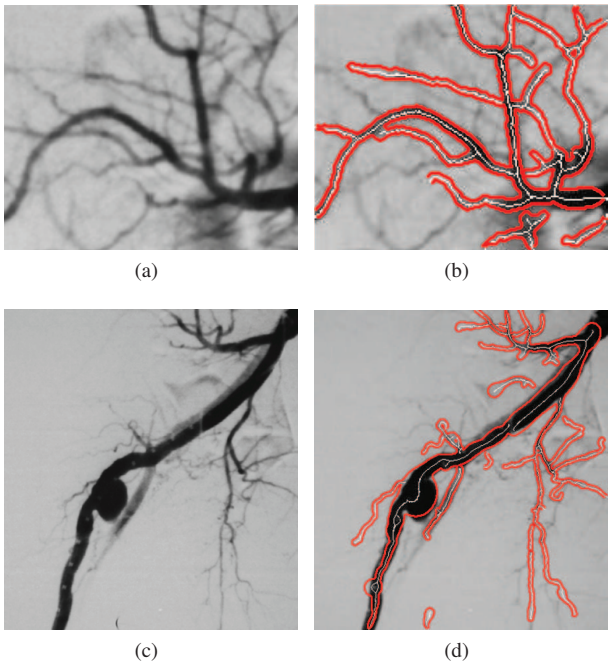


Fig. 6: Two examples of centerlines extracted from the medialness map $\mathcal{M}$ and their corresponding vessel segmentation, on 2D X-ray angiographies.

6. REFERENCES

[1] Xu, C. and Prince, J.L., "Snakes, Shapes, and Gradient Vector Flow," *IEEE Transactions on Image Processing*, vol. 7, no. 3, pp. 359–369, 1998.

[2] Xu, C. and Prince, J.L., "Generalized Gradient Vector Flow External Forces for Active Contours," *Signal Processing*, vol. 71, no. 2, pp. 131–139, 1998.

[3] Bauer, C., Bischof, H. and Beichel, R., "Segmentation of Airways Based on Gradient Vector Flow," *International Workshop on Pulmonary Image Analysis (MICCAI'09)*, pp. 191–201, 2009.

[4] Engel, D. and Curio, C., "Scale-invariant Medial Features Based on Gradient Vector Flow Fields," *Proc. of ICPR'08*, pp. 1–4, 2008.

[5] Bauer, C., *Segmentation of 3D Tubular Tree Structures in Medical Images*, Ph.D. thesis, Graz University of Technology, 2010.

[6] Yu, Z. and Bajaj, C., "A Segmentation-Free Approach for Skeletonization of Gray-Scale Images via Anisotropic Vector Diffusion," *Proc. of CVPR'04*, vol. 1, pp. 415–420, 2004.

[7] Hassouna, M.S. and Farag, A.A., "On the Extraction of Curve Skeletons using Gradient Vector Flow," *Proc. of ICCV'07*, pp. 1–8, 2007.

[8] Boukerroui, D., "Efficient Numerical Schemes for Gradient Vector Flow," *Proc. of ICIP'09*, pp. 4057–4060, 2009.

[9] Aylward, S., Pizer, S., Eberly, D. and Bullitt, E., "Intensity ridge and widths for tubular object segmentation and description," *Proc. of MMBIA'96*, pp. 131–139, 1996.